Hypertension

ORIGINAL ARTICLE

Redefining AT1 Receptor PET Imaging: Introducing the Radiotracer [^{18}F]DR29

Xinyu Chen, Hiroyuki Kimura, Takanori Sasaki, Konrad Klimek, Saskia Mühlig, Anahi Paula Arias-Loza, Naoko Nose, Yusuke Yagi, Steven P Rowe, Constantin Lapa, Rudolf A. Werner*, Takahiro Higuchi*

BACKGROUND: AT1R (angiotensin II type 1 receptors) are central to the renin-angiotensin system and are involved in regulating blood pressure and renal physiology. This study introduces [^{18}F]DR29, a fluorine-18-labeled radiotracer for positron emission tomography imaging, to enable noninvasive visualization of AT1R expression. Its potential applications in understanding AT1R-associated renal processes are explored in healthy and hypertensive rat models.

METHODS: Radiolabeling was established, and biodistribution studies were conducted on healthy Wistar rats with and without the AT1R antagonist candesartan and transporter inhibitors. Dynamic positron emission tomography imaging assessed tracer specificity, and feasibility for renal AT1R quantification was explored using a hypertensive rat model.

RESULTS: [^{18}F]DR29 was radiolabeled with a yield of 36±6%. High kidney uptake was observed, significantly reduced by candesartan (kidney-to-blood ratio, 0.43±0.01 versus 4.54±1.59 in vehicle, where vehicle refers to saline without any treatment). Transporter inhibition protocols targeting organic anion transporting polypeptides (liver) and organic anion transporters (kidneys) successfully reduced radiotracer clearance, increasing the specific accumulation of [^{18}F]DR29 in the kidneys and improving renal imaging contrast. Positron emission tomography imaging revealed rapid kidney uptake and stable retention over 2 hours. In hypertensive rats, kidney uptake was higher, aligning with AT1R expression levels.

CONCLUSIONS: These results support [^{18}F]DR29 as a promising tool for the noninvasive evaluation of renal AT1R expression in healthy and diseased states. The findings lay the groundwork for clinical translation, offering potential applications in diagnosing and managing kidney-related diseases, including hypertension and other conditions involving AT1R dysregulation.
***(Hypertension.* 2025;82:00–00. DOI: 10.1161/HYPERTENSIONAHA.124.24441.)** • **Supplement Material**.

Key Words: angiotensin II type 1 receptor ■ organic anion transporters ■ organic anion transporting polypeptides ■ renal imaging ■ renin-angiotensin system

The renin-angiotensin system (RAS) orchestrates crucial regulatory functions across multiple physiological systems, prominently influencing cardiovascular and renal health. Its cascade involves the conversion of angiotensinogen to angiotensin I by renin, with subsequent conversion to angiotensin II via ACE (angiotensin-converting enzyme). AT1R (angiotensin II type 1 receptor) exerts diverse effects including vasoconstriction, inflammation, and fibrosis, pivotal in the pathogenesis of various renal diseases. While clinical interventions targeting the RAS, such as ACE inhibitors and AT1R antagonists, have demonstrated efficacy in managing hypertension, their precise dosing strategies remain under scrutiny, particularly in renal pathologies.[1]

Molecular imaging techniques, notably positron emission tomography (PET), offer promising avenues by targeting specific molecular pathways such as AT1R, enabling precise visualization and quantification of

Correspondence to: Takahiro Higuchi, Department of Nuclear Medicine and Comprehensive Heart Failure Center, University Hospital Würzburg, Oberdürrbacher Str. 6, 97080 Würzburg, Germany. Email thiguchi@me.com
*R.A. Werner and T. Higuchi contributed equally.
Supplemental Material is available at https://www.ahajournals.org/doi/suppl/10.1161/HYPERTENSIONAHA.124.24441.
For Sources of Funding and Disclosures, see page XXX.

Hypertension is available at www.ahajournals.org/journal/hyp

NOVELTY AND RELEVANCE

What Is New?

This study introduces [^{18}F]DR29, a novel fluorine-18-labeled positron emission tomography (PET) radiotracer designed for noninvasive imaging of renal AT1R (angiotensin II type 1 receptors) expression, featuring enhanced stability and specificity.

What Is Relevant?

The radiotracer [^{18}F]DR29 demonstrates clear renal AT1R visualization by overcoming challenges posed by off-target uptake, highlighting its value in studying hypertension and renal pathophysiology.

Clinical/Pathophysiological Implications?

The ability of [^{18}F]DR29 to noninvasively quantify AT1R expression offers a pathway to precision medicine, enabling tailored antihypertensive therapies based on individual receptor profiles. This approach could optimize medication selection and dosing, improving treatment efficacy while minimizing side effects in patients with hypertension and other AT1R-related conditions.

Nonstandard Abbreviations and Acronyms

ACE	angiotensin-converting enzyme
AT1R	angiotensin II type 1 receptor
HPLC	high performance liquid chromatography
NTZ	nitazoxanide
OATP	organic anion transporting polypeptide
OAT	organic anion transporter
PET	positron emission tomography
RAS	renin-angiotensin system
RIF	rifampicin
SUV	standardized uptake value

receptor expression in renal tissues. Fluorine-18 labeling radiotracers targeting AT1R represent a novel approach to elucidating renal disease pathophysiology, facilitating early detection, characterization, and therapeutic monitoring.

To date, a limited array of PET radiotracers has been documented in the literature,[2–5] among which [^{11}C]KR31173,[6] developed from the AT1R selective antagonist SK-1080 with subnanomolar IC_{50} values,[7] demonstrates efficient radiolabeling protocols.[2,8] Nevertheless, the practical application of [^{11}C]KR31173 is constrained by the brief half-life of carbon-11 (20 minutes). In contrast, drawing from our research group's expertise in developing radiotracers derived from clinically utilized AT1R antagonists,[4,5] the introduction of fluorine-18 (half-life 110 minutes) at the α-position of the aliphatic chain on the heterocyclic ring of sartans has emerged as a viable strategy. This modification maintains target affinity, while maintaining the lipophilicity and ensuring satisfactory radiolabeling yield and in vivo stability against defluorination.

Recent studies such as those using [^{11}C]KR31173 in pig models with renovascular hypertension[9] and [^{18}F]FPyKYNE-losartan in kidney disease models[10,11] have demonstrated their effectiveness. These radiotracers not only indicate increased AT1R binding in pathological conditions but also show potential in understanding chronic kidney disease and cardiovascular pathologies.[2,12,13] In addition, emerging evidence suggests a comprehensive role of the RAS in tumor development and progression. Using AT1R-targeting radiotracers in PET enables a quantitative assessment of AT1R distribution, providing a novel approach for prognostic evaluation of tumor cell migration.

The current study focuses on the new generation F18-labeled AT1R-targeting radiotracer [^{18}F]DR29. The design is based on the structural framework of SK-1080, chosen for its high binding affinity and stability in vivo. This base structure was further optimized to enhance the radiotracer's performance by incorporating a fluorination approach that allows for high-yield radiolabeling and prevents defluorination during biological processes. These design choices ensure that [^{18}F]DR29 not only maintains strong affinity for AT1R but also exhibits excellent stability, leading to more reliable imaging results.

We will investigate its radiolabeling and characterization, analyze its biodistribution and dynamic PET imaging capabilities in rats. A particular focus will be placed on understanding the in vivo kinetics and predominant renal localization of [^{18}F]DR29, which can be attributed to the high physiological expression of AT1R in the kidneys. It is noteworthy that renal and hepatic uptake of [^{18}F]DR29 is also influenced by organic anion transporters (OATs) and organic anion transporting polypeptides (OATPs). These membrane proteins play a critical role in transporting various molecules, including drugs, across cell membranes. Therefore, evaluating the interaction between [^{18}F]DR29 and these transporters is essential for accurately interpreting the biodistribution and targeting efficiency observed in our experiments. In addition to the aforementioned, in vitro and in vivo stability assessments of [^{18}F]DR29 will be addressed to comprehensively describe the radiotracer's properties.

MATERIALS AND METHODS

The data that support the findings of this study are available from the corresponding author upon reasonable request. All experiments were conducted in strict accordance with the Guide for the Care and Use of Laboratory Animals, published by the U.S. National Institutes of Health,[14] Guidance for Methods Description Used in Preclinical Imaging Papers, and the ARRIVE guidelines.[15] Experimental protocols were approved by the Animal Ethics Committee of the National Cerebral and Cardiovascular Center, Research Institute, Osaka (Approval number 18019), and Okayama University, Okayama (Approval number: OKU-2024488), Japan.

Radiochemistry

The radiolabeling was conducted in accordance with methods previously outlined in our research.[5] In brief, [^{18}F]fluoride (typically started from 2 GBq) was eluted from a Waters Sep-Pak Accell Plus QMA Plus Light cartridge (Waters GmbH, Eschborn, Germany) using a methanol/water solution of potassium carbonate (2.5 µmol) and Kryptofix 222 (5 µmol), then azeotropically dried at 110 °C for 10 minutes, with an additional 6 minutes after adding anhydrous acetonitrile (600 µL). A solution of the precursor (1 mg) in anhydrous acetonitrile (200 µL) was heated at 120 °C for 10 minutes. After solvent removal at 100 °C under nitrogen, the residue was treated with 4M HCl (250 µL in water/dioxane, 4:1, v/v) and heated at 120 °C for 10 minutes (Figure 1A). The reaction solution was purified via a high-performance liquid chromatography (HPLC) system equipped with a COSMOSIL 5C$_{18}$-ARII column (5 µm, 6.0 ID×150 mm). Mobile phase: (A) water with 0.1% trifluoroacetic acid; (B) acetonitrile with 0.1% trifluoroacetic acid; flow rate 2.0 mL/min; isocratic at 35% of phase B. The [^{18}F]DR29 fraction (9.9 min) was collected, diluted with 15 mL 10% acetonitrile/water, and trapped on a preconditioned Waters Sep-Pak C18 Plus Light cartridge (Waters GmbH, Eschborn, Germany). After washing with 5 mL water, the product was eluted with 0.6 mL ethanol. The solvent was removed under nitrogen flow and the residual was diluted with saline for further use. The radiochemical identity, purity, and molar activity of the target radiotracer were determined using a COSMOSIL 5C$_{18}$-ARII column (5 µm, 4.6 ID×150 mm), flow rate 1.5 mL/min; with a gradient of 10% to 80% mobile phase B in 13 minutes (retention time 8.25 minutes).

Competitive Membrane Binding Assay

Angiotensin AT1R (human) membrane preparations in CHO-K1 cells (0.6 µg protein diluted in 50 mmol/L Tris·HCl buffer, $MgCl_2$ 5 mmol/L, pH 7.4; Revvity GmbH, Hamburg, Germany) were incubated with 20 KBq tracer or buffer and varying concentrations of angiotensin II or irbesartan at 37 °C for 60 minutes (200 µL total volume). After gently mixing, the preparation was applied to presoaked filtermates (150 µL 0.5% BSA in Tris·HCl, 10 minutes before application) in a manifold, followed by vacuum filtration and 15 washes with 150 µL ice cold Tris buffer. Filters were replaced into Eppendorf tubes and measured in a gamma counter (PerkinElmer 2480 WIZARD^2, PerkinElmer GmbH, Rodgau, Germany).

Animal Model

For the initial evaluation of the radiotracer, male Wistar rats (450–550 g, Charles River Laboratories) were used. Hypertensive disease model male SHR/Izm rats and the corresponding normotensive male WKY/Izm rats (280–360 g, ≈12 weeks old) were purchased from SLC (Japan SLC, Inc, Shizuoka, Japan).

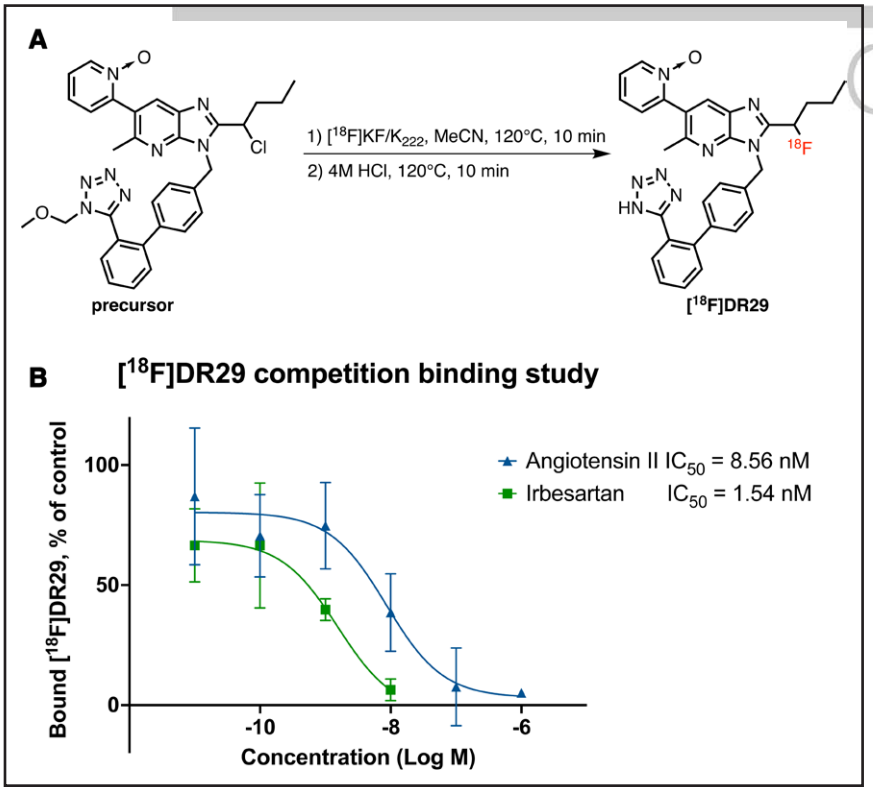

Figure 1. A, Radiolabeling of [^{18}F]DR29 with a 1-pot 2-steps labeling protocol from a α-chloride precursor with methoxymethyl protection at tetrazole ring.
B, Competitive AT1R (angiotensin II type 1 receptors) membrane binding assay using [^{18}F]DR29 against angiotensin II and irbesartan. The *y* axis label represents the percentage of [^{18}F]DR29 bound to the membrane under different inhibition conditions relative to the control (untreated condition without any inhibition). Both angiotensin II and irbesartan show almost identical IC_{50} values as reported,[8] demonstrating successful structural design of the radiotracer.

Anesthesia was induced and maintained during the experiment with 2% isoflurane vaporized with oxygen.[16] The respiratory rate of the ventilator was monitored and kept in the normal range throughout the imaging sessions using an anesthesia station (Apollo, Drägerwerk AG & Co. KGaA, Lübeck, Germany). Supplemental Material provided details of animal blood pressure measurements, demonstrating significantly higher systolic and diastolic blood pressures in SHR/Izm rats than in WKY/Izm rats. (Figure S1). Protocols for immunohistochemical staining and Western blot analysis from kidney tissues of both WKY/Izm and SHR/Izm rats are also provided in the Supplemental Material. The spontaneously hypertensive rat (SHR/Izm), a well-established model for studying primary hypertension, was derived from outbred Wistar Kyoto rats in the 1960s. This model is widely used due to its genetic predisposition to elevated blood pressure,[17,18] closely mimicking human essential hypertension, and was selected for its relevance in exploring the pathophysiological mechanisms of renal AT1R expression in hypertension.

PET Imaging and Biodistribution

Blocking Protocol

Nitazoxanide (NTZ, 250 mg/kg, suspension in water, oral, 2 hours prior) was used to inhibit OATs,[19] rifampicin (RIF, 10 mg/kg, lyophilized powder dissolved in sterile water for injection, intravenous, 10 minutes prior) was used to inhibit OATPs,[20] and candesartan (25 mg/kg, dissolved in DMSO and diluted with saline, intravenous, 10 minutes prior) served as an AT1R-specific blocker, minimizing interference with target specificity evaluation. For PET imaging in both healthy rats and hypertensive rat models, the NTZ+RIF blocking protocol was applied to all the animals to inhibit the unspecific uptake of [^{18}F]DR29. In biodistribution studies, 4 different protocols were applied to healthy rats: (1) Vehicle (saline without any treatment), (2) NTZ blocking, (3) NTZ+RIF, and (4) NTZ+RIF+candesartan. In hypertensive rat models, all animals were studied using the NTZ+RIF blocking protocol to exclude the unspecific uptake. Graphic flowcharts for PET imaging and biodistribution studies are provided in the Supplemental Material (Figures S2 and S3).

Animal Numbers

Wistar rats were used in the following numbers: n=2 per group (control and candesartan) for PET imaging; n=3 per group (Vehicle and NTZ) and n=4 per group (NTZ+RIF and NTZ+RIF+candesartan) for biodistribution studies. For hypertensive model SHR/Izm and corresponding normotensive WKY/Izm rats, n=2 per group were used for PET imaging; n=5 per group were used for biodistribution studies.

Biodistribution Studies

In biodistribution studies, animals under anesthesia were euthanized 60 minutes post-radiotracer administration (0.5–1 MBq). Organs of interest were harvested and weighed, and the radioactivity of each organ was measured in a gamma counter. Results are expressed as the percentage of injected dose per gram of tissue (%ID/g), adjusted for decay and normalized to organ weight. Finally, organ-to-blood ratios were calculated by dividing the %ID/g of each organ by that of blood.

Imaging Protocol

PET imaging was performed using a microPET FOCUS 120 system (Siemens, Erlangen, Germany). A 120-minute dynamic scan was initiated immediately after intravenous administration of the radiotracer (30–40 MBq) into the tail vein via bolus. The acquired list-mode data were transformed into 3-dimensional reconstructions, then re-binned with full 3-dimensional binning for dynamic image generation. The reconstructed images were analyzed using AMIDE imaging software (version 1.0.1). Tissue uptake was quantified as standardized uptake values (SUVs), from which time-activity curves of the liver and kidneys were generated with transmission computed tomography images for anatomic correlation.

Stability Studies

To evaluate the in vitro stability of the radiotracer in its injection formulation (an ethanol solution diluted with saline), the solution was analyzed by HPLC after incubating at room temperature for 0, 30, 60, and 120 minutes. The in vivo stability of [^{18}F]DR29 was assessed utilizing whole blood samples, collected 120 minutes post-radiotracer injection from animals subjected to PET imaging studies. Following euthanasia, whole blood was immediately extracted and anticoagulated with heparin. Aliquots of 1 mL each were then dispensed into 1.5 mL Eppendorf tubes containing 500 µL of acetonitrile. The mixtures were vortexed for homogenization and subsequently centrifuged at 3000 rpm for 5 minutes. The resultant supernatants, ≈500 µL each, were transferred into new Eppendorf tubes containing 100 µL of 10% trifluoroacetic acid aqueous solution. A subsequent centrifugation at 13 400 rpm for 5 minutes was performed. The final supernatants were then filtered through a 0.22 µm filter for HPLC analysis. The analytical methodology used for these assessments was consistent with the quality control procedures described above.

Statistics

All results are presented as the mean±SD. For all data sets, normality test using Shapiro-Wilk test were first performed before further statistical analysis. The detailed results of the normality tests, conducted due to the small sample sizes before performing parametric analyses, are provided in the Supporting Information (Tables S1 and S2). For comparisons of biodistribution data and liver/kidney-to-blood ratios under different blocking conditions, after confirming the normality of the data obtained from healthy Wistar rats, we applied ordinary 1-way ANOVA followed by Bonferroni's test for multiple comparisons. Similarly, after confirming normality in the SUV data from biodistribution studies, we used 2-way ANOVA followed by Bonferroni test to compare differences in blood and kidney SUVs between healthy (WKY/Izm) and hypertensive (SHR/Izm) rats. For Western blot analysis, an unpaired and 2-tailed *t* test was performed to compare the AT1R expression in kidney tissues. A *P* value of <0.05 was assumed to be statistically significant. Statistical analysis was performed with GraphPad Prism (version 10.2.3 GraphPad Software, San Diego).

RESULTS

Radiochemistry

Radiofluorination followed by deprotection was executed with slight modifications to a previously established

protocol.[4,5] Notably, due to the enhanced stability of the methoxylmethyl group, hydrochloric acid was added after removing the acetonitrile from postradiofluorination solution. In addition, 20% dioxane was incorporated into the deprotection solution instead of using a purely aqueous hydrochloric acid solution to improve the solubility of the highly lipophilic intermediate. These changes resulted in a 9% radiochemical yield improvement, preventing the loss of radioactivity. Moreover, due to the small, flexible fluorine atom, chiral C to F stereoisomers were not separated after radiolabeling. This flexibility prevented effective differentiation between the isomers, which likely possess identical affinity at AT1R, rendering separation unnecessary. An HPLC method to purify the final product was developed, specifically to remove the chloride byproduct from the extra precursor (Figure S4). Consequently, [^{18}F]DR29 was synthesized with a typical 2 GBq starting radioactivity, in <90 minutes labeling time, and a radiochemical yield of 36±6% (n=5, decay-corrected) while maintaining a radiochemical purity of >99% (Figure S6). The molar activity achieved ranged between 1.9 and 5.1 GBq/μmol.

Competitive Membrane Binding Assay

Angiotensin II, the endogenous substrate of AT1R, and the selective AT1R antagonist irbesartan were evaluated while using [^{18}F]DR29 as the radioligand. Both compounds show high affinities at AT1R, with angiotensin II at 8.56 nmol/L and irbesartan 1.54 nmol/L, respectively (Figure 1B)—almost identical to affinities previously reported.[5]

PET Imaging and Biodistribution in Healthy Rats

Biodistribution studies of [^{18}F]DR29 demonstrated that blocking OATs and OATPs impacted tracer distribution and pharmacokinetics by reducing hepatic excretion and increasing renal uptake, with AT1R specificity confirmed by candesartan. In initial studies using [^{18}F]DR29 without any blocking protocol (Figure 2A), moderate kidney uptake (2.79±0.70 %ID/g) could be observed in contrast to pronounced hepatic (6.38±1.23 %ID/g) and subsequent excretion into the intestinal tract (5.55±0.92 %ID/g), possibly mediated by OATPs.[21] Following the inhibition of OATs in the kidneys with nitazoxanide, a noticeable decrease in renal uptake was observed (Figure 2A), while liver excretion into the intestine increased twofold. Conversely, when both OATs and OATPs were blocked (Figure 2A NTZ+RIF), a decrease in radioactivity in both liver (3.95±1.61 %ID/g) and intestine (2.33±1.16 %ID/g) was noted, alongside with an increase in renal uptake (5.10±1.69 %ID/g). This renal increase was specifically attenuated by candesartan (0.32±0.13 %ID/g, $^{****}P<0.0001$, n=4), without affecting uptake in other major organs except for the adrenal gland, whose function, specifically regulated by AT1R, is crucial for blood pressure regulation. Adrenal uptake also decreased significantly following candesartan treatment, from 0.64±0.28 %ID/g to 0.15±0.07 %ID/g ($^{**}P<0.01$, n=4; Figure 2A NTZ+RIF+candesartan). Notably, the radiotracer distribution in the blood pool increased slightly following the dual blockage, likely due to the inhibited excretion from both liver and kidneys. When converted into organ-to-blood ratios, the kidneys exhibited the highest uptake (with an organ-to-blood ratio of 4.54±1.59) compared with the liver (3.42±0.80) following the dual blockage (Figure 2B and 2C, NTZ+RIF). The blocking study with candesartan significantly diminished renal uptake (0.43±0.01, Figure 2C, $^{**}P<0.01$, n=4), while the uptake in the liver remained stable (2.93±0.54, Figure 2C, ns, n=4).

In PET imaging, the hepatic uptake via OATPs and renal excretion via OATs were inhibited using rifampicin and nitazoxanide, respectively. Pretreatment by AT1R antagonist candesartan before radiotracer injection significantly reduced the renal uptake (Figures 3 and 4). In dynamic imaging, a rapid and distinct renal uptake, particularly in the cortical area, was observed just 2 min after the injection of [^{18}F]DR29. This high tissue contrast persisted for the entire 2-hour duration of the scan (Figure 4A). The specific blocking study, based on the injection of the selective AT1R blocker candesartan 10 minutes before the tracer administration, showed a significantly reduced renal uptake (Figure 3), whereas the uptake in other organs remained unchanged. Time-activity curves derived from dynamic PET images also reflect the above results. Under the condition of OATPs and OATs blockage, which served as a control, the renal uptake of [^{18}F]DR29 rapidly plateaued within <10 minutes post-injection, but exhibited slow clearance. The SUV in the kidney peaked at 30 to 40 minutes (5.22±1.50), and remained elevated at 120 minutes post-injection (3.44±0.82). This level was significantly higher than the SUV in the blood pool at the same time point (1.15±0.08). In contrast, following pretreatment with the AT1R-selective inhibitor candesartan, the renal uptake paralleled the blood pool level throughout the measurement period. The SUV for renal uptake at both 60 and 120 minutes post-injection was markedly lower under candesartan blockage (0.42±0.27 and 0.33±0.13, respectively) compared with the control condition (4.80±1.33 and 3.44±0.82, respectively) at the same time point. Meanwhile, liver uptake displayed minimal change, with no significant difference observed between conditions with and without candesartan blockage (Figure 4B).

PET Imaging and Biodistribution in Hypertensive Rat Models

PET imaging of [^{18}F]DR29 at 30 to 60 minutes post-injection in hypertensive rat models revealed higher

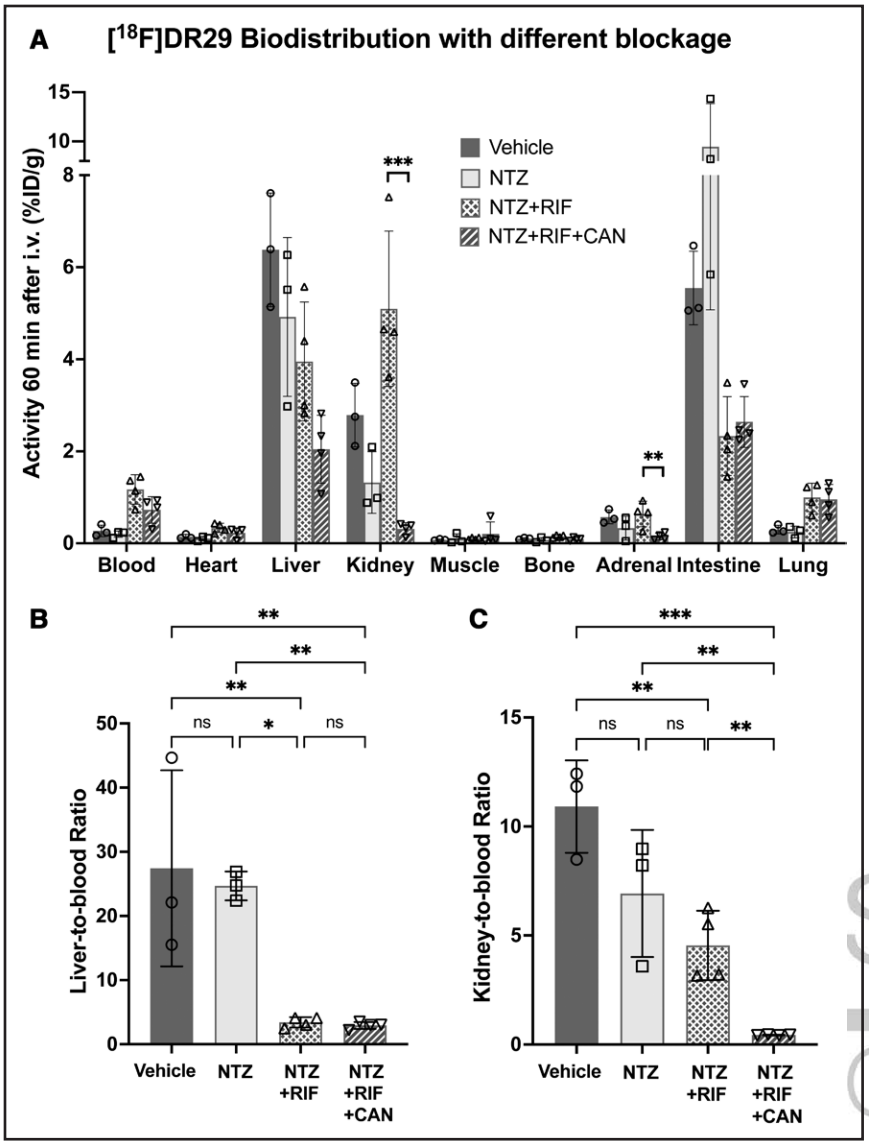

Figure 2. A, Biodistribution of [18F] DR29 in healthy rats 60 minutes post-injection in organs of interest under different blocking conditions. Vehicle represents injection of saline without any further treatment. Following blockade of organic anion transporting polypeptides (OATPs) by rifampicin (RIF, 10 mg/kg, intravenous) and organic anion transporters (OATs) by nitazoxanide (NTZ, 250 mg/kg, oral), a specific reduction in renal (****$P<0.0001$, n=4) and adrenal uptake (**$P<0.01$, n=4) blocked by candesartan (CAN, 25 mg/kg, intravenous) was observed, demonstrating AT1R (angiotensin II type 1 receptors) specificity. **B** and **C**, Organ-to-blood ratios of [18F]DR29 uptake in liver and kidneys following sequential blockade of OATs (NTZ), OATPs (RIF), and (AT1R, CAN). A significant reduction in kidney-to-blood ratio was observed after AT1R blockade by CAN (**$P<0.01$, n=4), while the liver-to-blood ratio remained unchanged, consistent with dynamic positron emission tomography (PET) imaging results. Data are presented as mean±SD (n=3 for Vehicle and NTZ group, n=4 for NTZ+RIF and NTZ+RIF+CAN group). After confirmation of the normality of data sets, 1-way ANOVA was performed, followed by Bonferroni post hoc test for multiple comparisons. *$P<0.05$; **$P<0.01$; ***$P<0.001$; *ns*, no significant difference.

renal uptake in the hypertensive (SHR/Izm) compared with the normotensive (WKY/Izm) rats, whereas no noticeable changes were observed in liver uptake and the biliary excretion. Consistent with this finding, biodistribution analysis 60 minutes post-injection showed a significant increase ($P<0.01$) of radiotracer uptake in the kidneys of hypertensive rats (SHR/Izm) compared with normotensive ones (WKY/Izm), while blood levels in both models showed no significant difference (Figure 5A). Immunohistochemical staining of kidneys sections confirmed the increased AT1R expression in hypertensive (SHR/Izm) rats compared with normotensive (WKY/Izm) ones, with higher fluorescence intensity in the renal cortex. Control experiments without the primary antibody were performed under identical acquisition settings, and the resulting images for both WKY/Izm and SHR/Izm kidney sections are provided in the Supplemental Material (Figure S5). Western blot analysis of protein extracted from kidney tissues further confirmed a significant upregulation of AT1R expression in hypertensive (SHR/Izm) rats compared with normotensive (WKY/Izm) rats (n=4 per group, duplicate of each kidney sample, $P<0.05$). Quantification of AT1R protein levels, normalized to the internal standard Vinculin, revealed a 35% higher AT1R expression in SHR/Izm kidneys (Figure 5B). This finding is consistent with the observed differential expression in immunohistochemical sections and corroborates previous PET imaging and biodistribution studies using [18F] DR29.

Stability Studies

Stability studies confirmed that [18F]DR29 remains stable in its final formulation, which composed of ethanol and saline solution, over the entire 120-minute measurement period (Figure S6). Importantly, the presence of OATPs and OATs blockers, specifically rifampicin and

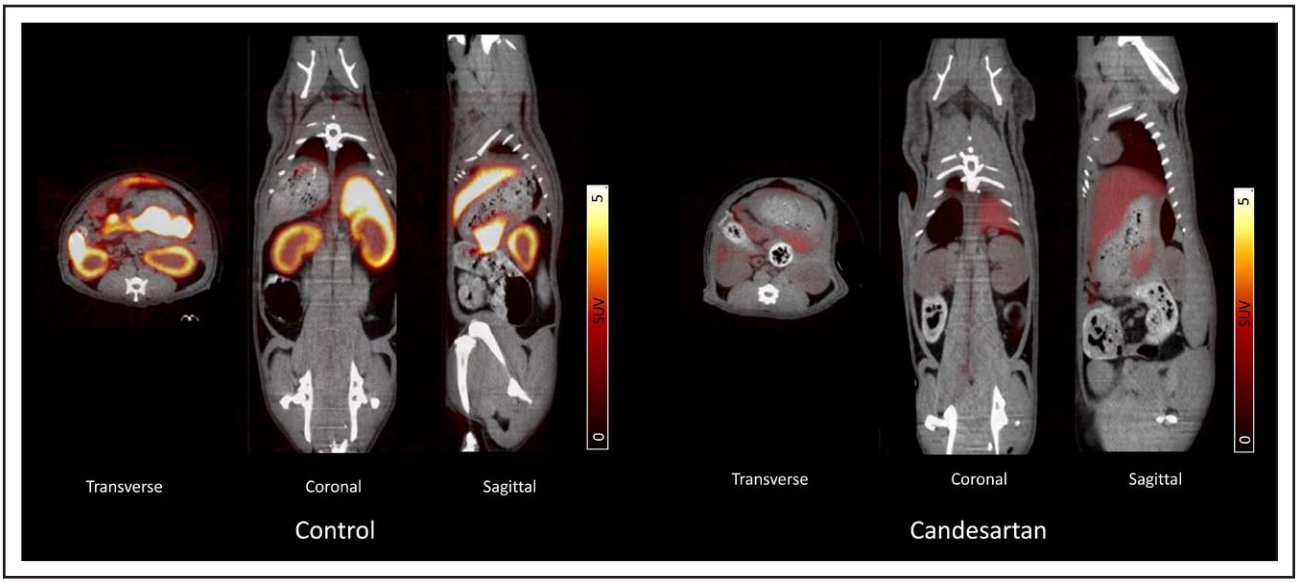

Figure 3. Comparison of [^{18}F]DR29 uptake via fused positron emission tomography (PET)/computed tomography (CT) images in rats under different blocking conditions, 50–60 minutes post-injection (n=2).
Control: Baseline uptake condition with off-target transport inhibition via nitazoxanide (NTZ) and rifampicin (RIF) pretreatment. Candesartan: Effect of additional angiotensin II type 1 receptor blockade by candesartan on uptake, under identical NTZ+RIF pretreatment. Pretreatment details: NTZ (organic anion transporter inhibitor, 250 mg/kg, oral) and RIF (organic anion transporting polypeptide inhibitor, 10 mg/kg, intravenous). SUV indicates standardized uptake value.

nitazoxanide, as well as the AT1R blocker candesartan, did not impact the stability of the radiotracer. Within the limits of our analytical HPLC method, neither free fluoride-18 nor significant metabolites were detected. This finding is further supported by biodistribution studies conducted 60-minute post-injection as well as dynamic PET imaging up to 120 minutes post-injection, both of which showed minimal bone uptake, indicative of low defluorination and good in vivo stability of the radiotracer. While low-pH reverse-phase HPLC conditions (due to the addition of trifluoroacetic acid) may not fully recover free fluoride,[22] the use of a broad 10% to 80% gradient method would have detected other potential metabolites, if present. Therefore, the absence of detectable hydrophilic or hydrophobic metabolites in whole blood samples 120 minutes post-injection provides strong evidence for the radiotracer's metabolic stability (Figures S7 and S8).

DISCUSSION

The current study investigated a new generation AT1R-targeted radiotracer [^{18}F]DR29 using PET technology. Initial radiolabeling was performed manually without optimization, achieving a radiochemical yield of 36±6%. While the molar activity was low due to a combination of low starting radioactivity and unavoidable carrier fluoride contamination during the synthesis, the results provided valuable initial insights. This efficiency enabled the transition to a cyclotron-automated module-based radiolabeling starting from a higher radioactivity production (>50-fold). Further evaluation using a competitive binding assay with AT1R membranes revealed nanomolar affinity of the radiotracer for AT1R, nearly identical to previously reported drugs, confirming the successful introduction of fluorine-18 at the α-position of the aliphatic chain through rational design. PET imaging and biodistribution studies in both healthy and hypertensive rats demonstrated the clinical potential of [^{18}F]DR29 for monitoring AT1R. Notably, the study achieved clear and specific AT1R imaging in the kidneys, with enhanced contrast facilitated by inhibition protocols targeting liver OATPs and kidney OATs. These protocols successfully reduced off-target uptake and increased the specific accumulation of [^{18}F]DR29 in the kidneys, further improving the quality of renal imaging. Findings from immunohistochemical staining and Western blot analysis of kidney tissues from hypertensive rat models are consistent with both PET imaging and biodistribution studies. This consistency further confirms the feasibility of AT1R imaging with this new tracer. Figure 6 summarizes the major transporters and receptors involved in the distribution of [^{18}F]DR29. While both OATPs and OATs are depicted in the liver, it is important to note that OATPs play a predominant role in hepatic uptake, whereas the contribution of OATs in the liver is comparatively minor. Therefore, the capacity of OATs in the liver was not considered in the current study.

Initial biodistribution studies and organ-to-blood ratios revealed that, without medication, the radiotracer primarily accumulated in the liver via OATPs (Figure 2), consistent with [^{11}C]KR31173.[2,23] This hepatic uptake

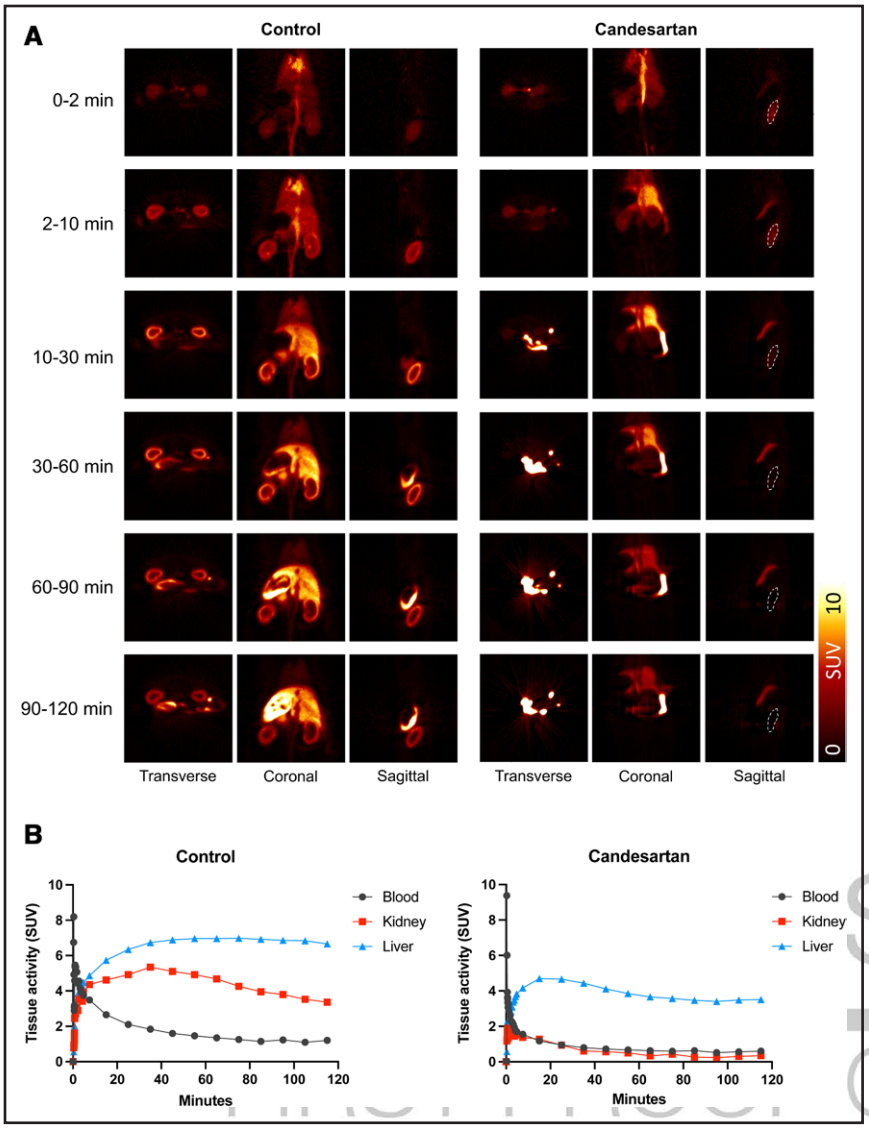

Figure 4. Pharmacokinetic profile and target specificity of [18F]DR29 in healthy Wistar rats.
A, Dynamic positron emission tomography (PET) imaging of healthy Wistar rats over a time-course of 120 minutes post-injection of [18F]DR29, providing a comprehensive depiction of its pharmacokinetic profile. Control: Baseline uptake condition with pharmacological blockade of hepatic organic anion transporting polypeptides (OATPs) by rifampicin (RIF, 10 mg/kg intravenous) and concurrent inhibition of renal organic anion transporters (OATs) by nitazoxanide (NTZ, 250 mg/kg, oral). Candesartan: Under identical NTZ+RIF pretreatment, it demonstrates the effect of additional angiotensin II type 1 receptor blockade with candesartan (CAN, 25 mg/kg intravenous). Note the significantly decreased kidney uptake (signal intensity within the white dotted line region in the Sagittal view), confirming target specificity. SUV, standardized uptake values. **B**, Time-activity curves of [18F]DR29 derived from the dynamic PET images for the Control and Candesartan with conditions described in (**A**). Uptake (mean SUV) in regions of interest (blood, liver, kidney) is shown (n=2 each group).

posed challenges for renal imaging aimed at AT1R, due to radioactivity scattering and spatial overlap with the intestines. Shimizu and coworkers proposed this issue and used [11C]telmisartan to investigate the transporting properties of OATP1B3 in the liver.[24]

OATPs and OATs are key transporters influencing the distribution and elimination of both endogenous and exogenous compounds, including drugs, toxins, and signaling molecules.[25] Unfortunately, their impact on radiotracer pharmacokinetics remains underexplored, which can be of critical relevance in the case of off-target uptake of theranostic radiopharmaceuticals.[26] Considering the fact that AT1R blockers are the substrate of both OATPs and OATs,[21,27] the current tracer, [18F]DR29, deriving from the AT1R-selective antagonist SK-1080, is expected to be taken up by OATPs in the liver and OATs in the kidneys,[27] contributing to off-target uptake. To address this, in the current studies, rifampicin, a nonselective OATP1B1/3 inhibitor[20] and was chosen as an inhibitor for OATP-targeted PET tracers.[28,29] Similarly, nitazoxanide was selected for nonselective OAT1/3 inhibition.[19] Pretreatment with rifampicin and nitazoxanide significantly reduced liver uptake, bringing it down to match kidney levels. The hepatic uptake has been suppressed for more than 5-fold in terms of liver-to-blood ratio (Figure 2B), allowing for improved renal imaging contrast. Further blocking studies using the AT1R-selective antagonist candesartan has demonstrated the specificity of [18F]DR29, as renal uptake dropped significantly (5-fold in terms of kidney-to-blood ratio) without affecting other organs (Figure 2). PET imaging using the same blocking protocol further validated these findings (Figures 3 and 4), showing rapid and sustainable renal uptake, which can be attributed to specific AT1R uptake in the absence of candesartan blockade (Figure 4B).

The successful application of [18F]DR29 in hypertensive rats suggests its potential for clinical use in monitoring AT1R, particularly in the context of hypertension. The increased radiotracer uptake observed in hypertensive

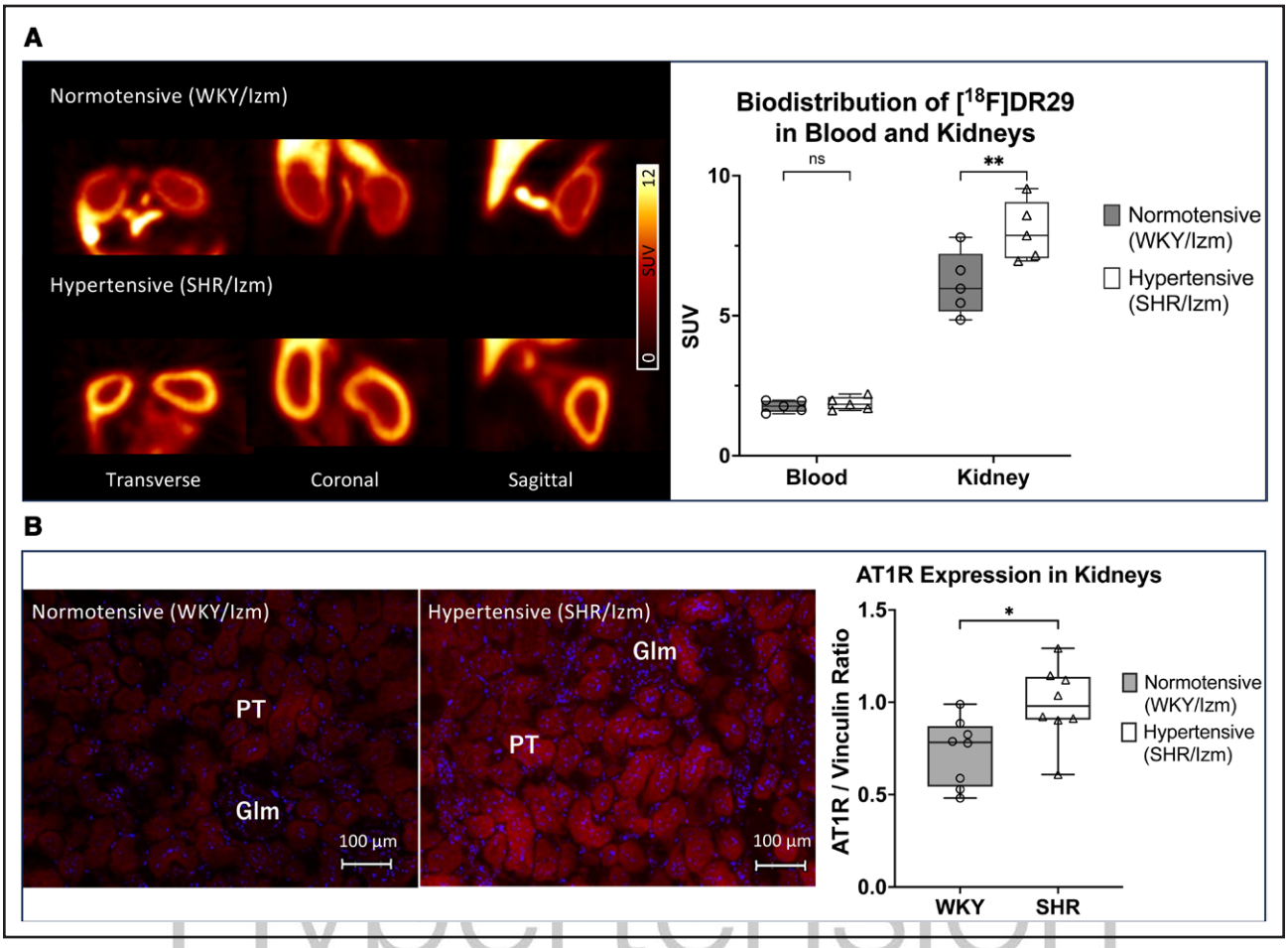

Figure 5. A, Static abdominal positron emission tomography (PET) images of normotensive (WKY/Izm) and hypertensive (SHR/Izm) rats acquired using the AT1R (angiotensin II type 1 receptors)-targeting radiotracer [18F]DR29 after a blocking protocol with nitazoxanide (NTZ) and rifampicin (RIF) to exclude unspecific uptake, 30–60 minutes post-injection (n=2 for PET imaging).

Tracer uptake in the kidneys of hypertensive rats (SHR/Izm) was notably increased compared with normotensive ones (WKY/Izm). Biodistribution analysis 60 minutes post-injection revealed a significant higher renal uptake in hypertensive rats (**P<0.01, n=5 per group for biodistribution studies), consistent with PET imaging results, highlighting the potential of [18F]DR29 for detecting AT1R upregulation in hypertensive conditions. Uptake in regions of interest, namely blood and kidney, is represented as standardized uptake value (SUV). After confirmation of the normality of data sets, a 2-way ANOVA followed by Bonferroni post hoc test for multiple comparisons test was performed. **P<0.01. **B**, AT1R expression in kidneys of normotensive (WKY/Izm) and hypertensive (SHR/Izm) rats. Immunohistochemical staining images of renal single axial sections depict AT1R fluorescence signals observed primarily in the proximal tubule (PT), with minimal labeling in the glomerulus (Glm). Magnification ×200, scale bar=100 µm. The fluorescent intensity from hypertensive one is higher than in normotensive rats, representing upregulated expression of AT1R. Furthermore, data from quantification of AT1R protein levels by Western Blot analysis, presented as the ratios of integrated density of AT1R over the internal standard Vinculin, also confirmed a significant upregulation of AT1R expression in the kidneys of SHR/Izm compared with WKY/Izm rats (n=4 per group, duplicate of each kidney sample). An unpaired t test was performed after confirmation of data normality.*P<0.05. ns indicates no significant difference.

kidneys, consistent with immunohistochemical staining and Western blot analysis that confirms elevated AT1R expression (Figure 5), signifies its ability to differentiate between healthy and diseased states. This could be instrumental in assessing AT1R expression levels in the kidneys noninvasively and tracking changes over time to monitor the effectiveness of antihypertensive drugs. Furthermore, [18F]DR29 could provide valuable insights into the progression of hypertension and its associated complications, potentially guiding the selection and dosage of antihypertensive medications for personalized treatment regimens. This personalized approach has the potential to optimize treatment efficacy and minimize unnecessary side effects.

Despite pretreatment with nonselective OATP and OAT inhibitors, residual uptake remained in the liver with continued biliary excretion. This likely reflects the high capacity or activity of other OATP subtypes in those organs, for example, OATP2B1[15] and OATP4C1.[30] Another phenomenon worth mentioning is that the kidney uptake increased in the OATPs and OATs double-blocking condition, which was observed in both biodistribution studies

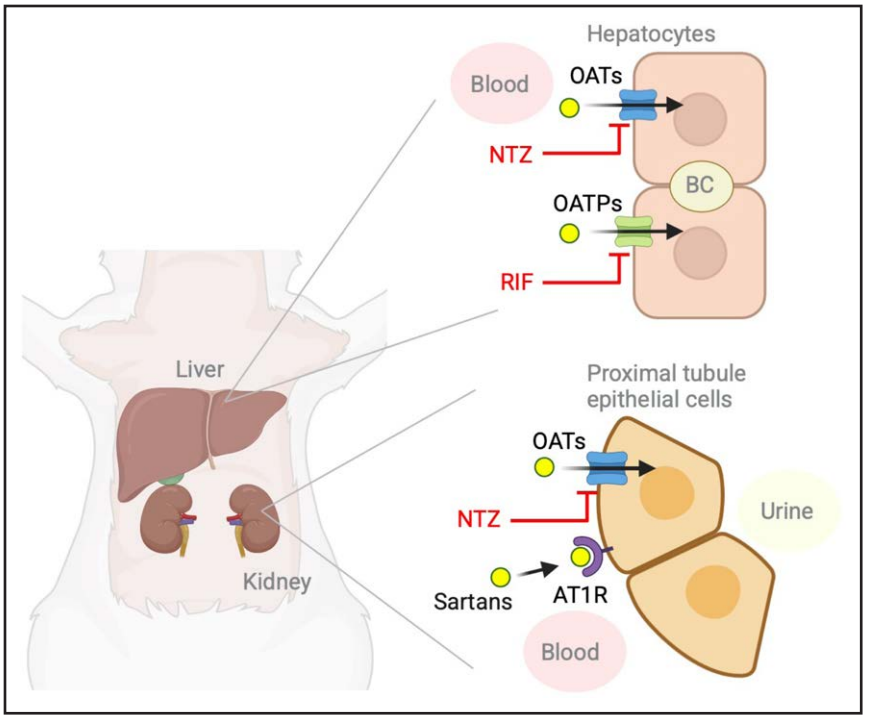

Figure 6. Illustration of distribution of transporters, their corresponding inhibitors, and AT1R (angiotensin II type 1 receptors) involved in the uptake of [^{18}F]DR29 in the current study.
Yellow spots represent either AT1R blockers sartans or AT1R-targeting radiotracers. BC indicates bile canaliculus; OATP, organic anion transporting polypeptide; OAT, organic anion transporter; RIF, rifampicin; and NTZ, nitazoxanide (created with BioRender.com).

and time-activity curves (Figures 2A and 4B). One explanation could be that, due to the blockage of OATPs in the liver and OATs in the kidney, blood counts of the radiotracer in circulation increased, which lead to enhanced accumulation in kidneys. Such an increase of the uptake in the kidney should be AT1R-mediated instead of a simple increase of blood activity, because it could be significantly diminished by candesartan blockage, with a drop of kidney-to-blood ratio from 4.54±1.59 to 0.43±0.01 (*P<0.05, Figure 2) and SUV from 4.80±1.33 to 0.42±0.27 (Figure 4B) at 60 minutes post-injection.

The observed increase in AT1R expression in the kidneys of hypertensive rats likely reflects a compensatory mechanism aimed at countering dysregulated blood pressure homeostasis. Hypertension induces sustained activation of the RAS, leading to elevated angiotensin II levels, which stimulate AT1R upregulation as part of a feedback loop to modulate renal vascular resistance and sodium reabsorption. This heightened receptor expression may enhance the kidneys' sensitivity to angiotensin II, exacerbating vasoconstriction and sodium retention, thereby perpetuating the hypertensive state. Physiologically, this overexpression signifies the kidneys' central role in the pathogenesis of hypertension and underscores the potential impact of targeted therapies. By quantifying AT1R expression, tools like [^{18}F]DR29 could provide critical insights into the extent of RAS activation, enabling precise adjustment of therapeutic regimens, such as AT1R blockers, to mitigate excessive receptor activity and restore renal and systemic homeostasis.

It should be noted that the target binding affinity, as well as in vivo kinetics, show great species and sex discrepancy. First, AT1R distribution and expression show species differences. [^{11}C]KR31173 showed higher specific AT1R uptake in the kidneys in baboons than in dogs,[23] whereas its myocardial retention in the healthy human heart is significantly lower than in pigs.[12] Similarly, [^{11}C]telmisartan demonstrated slower liver uptake in humans than in rats.[24] Second, the variation in OATPs and OATs across different species' organs leads to significant differences in off-target uptake and excretion. For instance, rodents lack OAT4, which is involved in the elimination of sartans from the kidneys,[31] unlike other species where OAT1 is predominantly expressed in the kidneys. In contrast, mice have a high abundance of OAT2.[32] This diversity implies that animal models, even within different rodent species, may not straightforwardly predict pharmacokinetics in other species. Although the underlying molecular mechanisms were not revealed, studies have shown that [^{18}F]FPyKYNE-losartan produces higher renal image contrasts and exhibits slower clearance from pig kidneys compared with rats.[3] Similarly, blocking studies of [^{11}C]KR31173 by pretreatment with SK-1080 showed a 49% reduction in kidney uptake in mice, but an 81% reduction in baboons,[23] further illustrating species-specific variations in tracer handling. Third, there are sex differences in the expression and function of OATs in rats. Studies have shown that the expression of OAT1 is higher in male than in female rats,[32] whereas the expression of OAT2 is vice versa. Those differences in the expression of OATs lead to higher nephrotoxicity of cisplatin in male than in female rats.[33] Fourth, even within the same species, age should also be considered. Research has revealed that overall, angiotensin II

receptors show a high expression in newborn rats, with AT2R as the predominant receptor, whereas in the adult conduction system, the total expression is dramatically reduced, with AT1R representing the major proportion.[34] Thus, due to the variations listed above, the comparison between results from different resources and the translation of preclinical findings to human pharmacokinetics should be done with caution.

The current research has significantly deepened our understanding of AT1R-targeted radiotracers off-target uptake and elimination via OATs and OATPs, enhancing the potential of PET imaging in assessing transporter-mediated drug-drug interactions.[35] It is conceivable that, by utilizing the same blocking protocol, alternative radiotracers designed to target AT1R could exhibit kinetics similar to those demonstrated in the present study. [^{18}F]DR29 has already exhibited promising attributes, including a high radiolabeling yield, enhanced in vivo stability, and substantial kidney uptake, rendering it a strong candidate for the current investigation. The relatively low molar activity of the tracer calls for a careful interpretation of the data, especially regarding its impact on biodistribution and specific uptake, underscoring the importance of methodological considerations in advancing the field.

PERSPECTIVES

The introduction of [^{18}F]DR29 as a novel AT1R-targeting PET radiotracer offers transformative potential for non-invasive renal imaging. By mitigating off-target uptake through OATP and OAT inhibition, [^{18}F]DR29 demonstrates high specificity and favorable pharmacokinetics, allowing accurate quantification of renal AT1R expression. This approach advances our understanding of AT1R's role in hypertensive pathophysiology and its associated renal processes. The successful application in hypertensive rat models underscores its clinical translational potential, particularly for differentiating healthy and diseased renal states. Looking forward, the deployment of [^{18}F]DR29 in larger animal studies and human trials could pave the way for precision diagnostics and therapeutic monitoring. Future investigations might explore its utility in other AT1R-associated conditions, such as chronic kidney disease or cardiovascular disorders, fostering a deeper integration of molecular imaging into personalized medicine.

ARTICLE INFORMATION

Received December 5, 2024; accepted July 9, 2025.

Affiliations

Nuclear Medicine, Faculty of Medicine, University of Augsburg, Germany (X.C., C.L.). Agency for Health, Safety and Environment, Kyoto University, Japan (H.K.). Faculty of Medicine, Dentistry and Pharmaceutical Sciences, Okayama University, Japan (T.S., N.N., Y.Y., T.H.). Goethe University Frankfurt, University Hospital, Clinic for Radiology and Nuclear Medicine, Department of Nuclear Medicine, Germany (K.K.). Department of Nuclear Medicine and Comprehensive Heart Failure Center (DZHI), University Hospital Würzburg, Germany (S.M., A.P.A.-L., T.H.). Department of Radiological Technology, Faculty of Medical Science, Kyoto College of Medical Science, Japan (Y.Y.). Molecular Imaging and Therapeutics, Department of Radiology, School of Medicine, University of North Carolina, Chapel Hill, NC (S.P.R.). Department of Nuclear Medicine, LMU Hospital, Ludwig-Maximilians-University of Munich, Germany (R.A.W.). Division of Nuclear Medicine and Molecular Imaging, The Russell H Morgan Department of Radiology and Radiological Science, Johns Hopkins University School of Medicine, MD (R.A.W.).

Acknowledgments

The authors gratefully acknowledge Dr Kenji Arimitsu, Dr Kaito Ohta, and Mr Masaru Akehi for their essential contributions to the chemistry and radiolabeling in this study. Their expertise was vital to the success of our research.

Sources of Funding

This study was funded by the German Research Council (DFG grants 507803309, R.A. Werner; 453989101, R.A. Werner, T. Higuchi; and 424778381, T. Higuchi) and was partially supported by the Okayama University RECTOR Program and a KAKENHI Grant (23K24288, T. Higuchi) from the Japan Society for the Promotion of Science (JSPS). The authors also extend their gratitude to the German Research Council for funding the U-SPECT5/CT E-class MILabs (INST 105022/90-1 FUGB).

Disclosures

R.A. Werner has received speaker honoraria from Novartis/AAA and PentixaPharm, reports advisory board work for Novartis/AAA and Bayer, and is involved in [68Ga]Ga-Pentixafor positron emission tomography (PET) Imaging in PAN Cancer (FORPAN), sponsored and planned by PentixaPharm. The other authors report no conflicts.

Supplemental Material

Protocols for Immunohistochemical Staining and Western Blot Analysis, Raw Data for Figures
Tables S1–S2
Figures S1–S8

REFERENCES

1. Flaten HK, Monte AA. The pharmacogenomic and metabolomic predictors of ACE inhibitor and angiotensin II receptor blocker effectiveness and safety. *Cardiovasc Drugs Ther.* 2017;31:471–482. doi: 10.1007/s10557-017-6733-2
2. Higuchi T, Fukushima K, Xia J, Mathews WB, Lautamäki R, Bravo PE, Javadi MS, Dannals RF, Szabo Z, Bengel FM. Radionuclide imaging of angiotensin II type 1 receptor upregulation after myocardial ischemia – reperfusion injury. *J Nucl Med.* 2010;51:1956–1961. doi: 10.2967/jnumed.110.079855
3. Hachem M, Tiberi M, Ismail B, Hunter CR, Arksey N, Hadizad T, Beanlands RS, deKemp RA, DaSilva JN. Characterization of 18F-FPy-KYNE-losartan for imaging AT1 receptors. *J Nucl Med.* 2016;57:1612–1617. doi: 10.2967/jnumed.115.170951
4. Chen X, Hirano M, Werner RA, Decker M, Higuchi T. Novel 18F-labeled PET imaging agent FV45 targeting the renin-angiotensin system. *ACS Omega.* 2018;3:10460–10470. doi: 10.1021/acsomega.8b01885
5. Hoffmann M, Chen X, Hirano M, Arimitsu K, Kimura H, Higuchi T, Decker M. 18F-Labeled derivatives of irbesartan for angiotensin II receptor PET imaging. *ChemMedChem.* 2018;13:2546–2557. doi: 10.1002/cmdc.201800638
6. Mathews WB, Yoo SE, Lee SH, Scheffel U, Rauseo PA, Zober TG, Gocco G, Sandberg K, Ravert HT, Dannals RF, et al. A novel radioligand for imaging the AT1 angiotensin receptor with PET. *Nucl Med Biol.* 2004;31:571–574. doi: 10.1016/j.nucmedbio.2003.10.014
7. Lee SH, Jung YS, Lee BH, Yun SI, Yoo SE, Shin HS. Characterization of angiotensin II antagonism displayed by SK-1080, a novel nonpeptide AT1-receptor antagonist. *J Cardiovasc Pharmacol.* 1999;33:367–374. doi: 10.1097/00005344-199903000-00004
8. Yoo SE, Kim SK, Lee SH, Yi KY, Lee DW. A comparison molecular field analysis and molecular modelling studies on pyridylimidazole type of angiotensin II antagonists. *Bio Med Chem.* 1999;7:2971–2976. doi: 10.1016/s0968-0896(99)00245-x
9. Xia J, Seckin E, Xiang Y, Vranesic M, Mathews WB, Hong K, Bluemke DA, Lerman LO, Szabo Z. Positron-emission tomography imaging of the angiotensin II type 1 receptor in swine renal artery stenosis. *Hypertension.* 2008;51:466–473. doi: 10.1161/HYPERTENSIONAHA.107.102715

10. Ismail B, deKemp RA, Hadizad T, Mackasey K, Beanlands RS, DaSilva JN. Decreased renal AT1 receptor binding in rats after subtotal nephrectomy: PET study with [18F]FPyKYNE-losartan. *EJNMMI Res*. 2016;6:55. doi: 10.1186/s13550-016-0209-4
11. Ismail B, deKemp RA, Croteau E, Hadizad T, Burns KD, Beanlands RS, DaSilva JN. Treatment with enalapril and not diltiazem ameliorated progression of chronic kidney disease in rats, and normalized renal AT1 receptor expression as measured with PET imaging. *PLoS One*. 2017;12:e0177451. doi: 10.1371/journal.pone.0177451
12. Fukushima K, Bravo PE, Higuchi T, Schuleri KH, Lin X, Abraham MR, Xia J, Mathews WB, Dannals RF, Lardo AC, et al. Molecular hybrid positron emission tomography/computed tomography imaging of cardiac angiotensin II type 1 receptors. *J Am Coll Cardiol*. 2012;60:2527–2534. doi: 10.1016/j.jacc.2012.09.023
13. Gulaldi NCM, Xia J, Feng T, Hong K, Mathews WB, Ruben D, Kamel IR, Tsui BMW, Szabo Z. Modeling of the renal kinetics of the AT1 receptor specific PET radioligand [11C]KR31173. *Biomed Res Int*. 2013;2013:1–12. doi: 10.1155/2013/835859
14. Committee for the update of the guide for the care and use of laboratory animals. *Guide for the care and use of laboratory animals*. 8th edition. The National Academies Press; 2011.
15. Kilkenny C, Browne W, Cuthill IC, Emerson M, Altman DG; NC3Rs Reporting Guidelines Working Group. Animal research: reporting in vivo experiments: the ARRIVE guidelines. *Br J Pharmacol*. 2010;160:1577–1579. doi: 10.1111/j.1476-5381.2010.00872.x
16. Chen X, Werner RA, Koshino K, Nose N, Mühlig S, Rowe SP, Pomper MG, Lapa C, Decker M, Higuchi T. Molecular imaging-derived biomarker of cardiac nerve integrity — introducing high NET affinity PET probe 18F-AF78. *Theranostics*. 2022;12:4446–4458. doi: 10.7150/thno.63205
17. Takeuchi F, Liang YQ, Isono M, Tajima M, Cui ZH, Iizuka Y, Gotoda T, Nabika T, Kato N. Integrative genomic analysis of blood pressure and related phenotypes in rats. *Dis Model Mech*. 2021;14:dmm048090. doi: 10.1242/dmm.048090
18. Aragane Y, Higashino T, Kinoshita K, Ashenagar MS, Higashino H. Hypertension-associated genes in the mesenteric artery of three spontaneously hypertensive rat substrains identified using a DNA array method. *Front Biosci (Landmard Ed)*. 2022;27:191. doi: 10.31083/j.fbl2706191
19. Duan P, Li S, Ai N, Hu L, Welsh WJ, You G. Potent inhibitors of human organic anion transporters 1 and 3 form clinical drug libraries: discovery and molecular characterization. *Mol Pharm*. 2012;9:3340–3346. doi: 10.1021/mp300365t
20. Karlgren M, Vildhede A, Norinder U, Wisniewski JR, Kimoto E, Lai Y, Haglund U, Artursson P. Classification of inhibitors of hepatic Organic Anion Transporting Polypeptides (OATPs): influence of protein expression on drug-drug interactions. *J Med Chem*. 2012;55:4740–4763. doi: 10.1021/jm300212s
21. Yamashiro W, Maeda K, Hirouchi M, Adachi Y, Hu Z, Sugiyama Y. Involvement of transporters in the hepatic uptake and biliary excretion of valsartan, a selective antagonist of the angiotensin II AT1-receptor, in humans. *Drug Metab Dispos*. 2006;34:1247–1254. doi: 10.1124/dmd.105.008938
22. Ory D, Van den Brande J, de Groot T, Serdons K, Bex M, Declercq L, Cleeren F, Ooms M, Van Laere K, Verbruggen A, et al. Retention of [18F]fluoride on reversed phase HPLC columns. *J Pharm Biomed Anal*. 2015;111:209–214. doi: 10.1016/j.jpba.2015.04.009
23. Zober TG, Mathews WB, Seckin E, Yoo SE, Hilton J, Xia J, Sandberg K, Ravert HAT, Dannals RF, Szabo Z. PET imaging of the AT1 receptor with [11C]KR31173. *Nucl Med Biol*. 2006;33:5–13. doi: 10.1016/j.nucmedbio.2005.08.005
24. Shimizu K, Takashima T, Yamane T, Sasaki M, Kageyama H, Hashizume Y, Maeda K, Sugiyama Y, Watanabe Y, Senda M. Whole-body distribution and radiation dosimetry of [11C]telmisartan as a biomarker for hepatic organic anion transporting polypeptide (OATP)1B3. *Nucl Med Biol*. 2012;39:847–853. doi: 10.1016/j.nucmedbio.2012.01.008
25. Roth M, Obaidat A, Bruno H. OATPs, OATs and OCTs: the organic anion and cation transporters of the SLCO and SLC22A gene superfamilies. *Br J Pharmacol*. 2012;165:1260–1287. doi: 10.1111/j.1476-5381.2011.01724.x
26. Bayer M, Kuçi Z, Schmömig E, Gründemann D, Dittmann H, handgretinger R, Bruchelt G. Uptake of mIBG and catecholamines in noradrenaline- and organic cation transporter-expressing cells: potential use of corticosterone for a preferred uptake in neuroblastoma- and pheochromocytoma cells. *Nucl Med Biol*. 2009;36:287–294. doi: 10.1016/j.nucmedbio.2008.12.010
27. Yamada A, Maeda K, Kamiyama E, Sugiyama D, Kondo T, Shiroyanagi Y, Nakazawa H, Okano T, Adachi M, Schuetz JD, et al. Multiple human isoforms of drug transporters contribute to the hepatic and renal transport of Olmesartan, a selective antagonist of the angiotensin II AT1-receptor. *Drug Metab Dispos*. 2007;35:2166–2176. doi: 10.1124/dmd.107.017459
28. Amor D, Goutal S, Marie S, Caillé F, Bauer M, Langer O, Auvity S, Tournier N. Impact of rifampicin-inhibitable transport on the liver distribution and tissue kinetics of erlotinib assessed with PET imaging in rats. *EJNMMI Res*. 2018;8:81. doi: 10.1186/s13550-018-0434-0
29. Yagi Y, Kimura H, Okuda H, Ono M, Nakamoto Y, Togashi K, Saji H. Evaluation of [18F]pitavastatin as a positron emission tomography tracer for in vivo organic anion transporter peptide. *Nucl Med Biol*. 2019;74-75:25–31. doi: 10.1016/j.nucmedbio.2019.08.001
30. Sato T, Mishima E, Mano N, Abe T, Yamaguchi H. Potential drug interactions mediated by renal organic anion transporter OATP4C1. *J Pharmacol Exp Ther*. 2017;362:271–277. doi: 10.1124/jpet.117.241703
31. Noguchi S, Okochi M, Atsuta H, Kimura R, Fukumoto A, Takahashi K, Nishimura T, Tomi M. Substrate recognition of renally eliminated angiotensin II receptor blockers by organic anion transporter 4. *Drug Metab Pharmacokinet*. 2021;36:100363. doi: 10.1016/j.dmpk.2020.10.002
32. Basit A, Radi Z, Vaidya VS, Karasu M, Prasad B. Kidney cortical transporter expression across species using quantitative proteomics. *Drug Metab Dispos*. 2019;47:802–808. doi: 10.1124/dmd.119.086579
33. Nematbakhsh M, Ebrahimian S, Tooyserkani M, Eshraghi-Jazi F, Talebi A, Ashrafi F. Gender difference in cisplatin-induced nephrotoxicity in a rat model: greater intensity of damage in male than female. *Nephrourol Mon*. 2013;5:818–821. doi: 10.5812/numonthly.10128
34. Bastien NR, Ciuffo GM, Saavedra JM, Lambert C. Angiotensin II receptor expression in the conduction system and arterial duct of neonatal and adult rat hearts. *Regul Pept*. 1996;63:9–16. doi: 10.1016/0167-0115(96)00012-2
35. Wulkersdorfer B, Wanek T, Bauer M, Zeitlinger M, Müller M, Langer O. Using positron emission tomography to study transporter-mediated drug-drug interactions in tissues. *Clin Pharmacol Ther*. 2014;96:206–213. doi: 10.1038/clpt.2014.70